Stochastic Simulations of Multiphase Flow and Contaminant Transport Associated with LNAPL Leakage

التمثيلات الإحصائية لتدفق السوائل وحركة الملوثات المرتبطة بتسرب السوائل الخفيفة الغير قابلة للذوبان في الماء

Khaled S. Abdel-Azeez[a], Ahmed E. Hassan[b] , Mohsen Ezzeldin[a]

[a] Irrigation and Hydraulics Department, Faculty of Engineering, Mansoura University.

[b] Irrigation and Hydraulics Department, Faculty of Engineering, Cairo University.

ملخص البحث:

تم إعداد نموذج عددي للتدفق المركب وانتقال الملوثات لدراسة تأثير عدم تجانس خواص التربة علي تسرب السوائل الخفيفة الغير ذائبة في الماء والملوثات الناتجة عنها الذائبة في الماء والمتطايرة في الهواء. يأخذ النموذج في الإعتبار عدم التجانس في التوصيلية الهيدروليكية ومسامية التربة ومتغيرات فان جنوختن المرتبطة بعلاقات درجة التشبع مع الضغط الشعري. تم وضع النموذج في اطار مونت كارلو الإحصائي والحل باستخدام فروض متعددة لعدم تجانس الطبقات. تمت دراسة تسعة حالات لعدم التجانس وسيناريوهات الإرتباط بين النفاذية ومسامية التربة ومتغيرات فان جنوختن. وجد من الدراسة أن عدم التجانس في نفاذية التربة له أكبر تأثير علي توزيع الملوثات الذائبة في الماء وتوزيع الملوثات المتطايرة في الهواء الأرضي وعلي كمياتها، يليه عدم التجانس في باقي المتغيرات وجد أن له تأثير ضعيف علي حركة السوائل والملوثات المتعلقة بها.

Abstract

A multiphase flow and transport numerical model is developed to study the leakage of light non-aqueous phase liquids (LNAPL) into the vadose zone and the associated contamination of both the unsaturated and saturated zones. The model is used to provide a better tool for addressing the movement and spreading of the NAPL phase and the resulting contamination in both the vadose zone and the saturated zone. In order to guide experimental design and field investigations, the model is used to evaluate the sensitivity of the results to various flow and transport parameters. It is found that the NAPL density and the capillary pressure parameters (van Genuchten parameters) increase the NAPL spreading in one direction at the expense of the spreading in the other direction. The remaining soil, flow, and transport parameters affect the vertical and lateral spreading in a similar manner. Based on the results presented herein, it seems that the exponent *m* of the van Genuchten capillary pressure-saturation relationship is the most influential parameter.

Keywords:

groundwater; multiphase flow; dissolved contaminants; volatilized contaminants

Introduction

Leakage of organic industrial liquids and petroleum derivatives into the subsurface is considered a major environmental problem due to the risk of long-lasting and wide-spreading contamination of both air and water. Dissolved and volatilized contaminants can transfer from these liquids to subsurface water and air, and thus these liquids are considered as a continuous source of contaminant. Great awareness of the multiphase flow of light non-aqueous phase liquids (LNAPL), water, and air in porous media has led to considerable works during the past few decades (e.g., Kaluarachchi and Parker 1989; Corapcioglu et al. 1996; Liao and Aral 2000; Kim and Corapcioglu 2001; Mendicino et al. 2006; Suk and Yeh 2007; just to name a few). Spatial variability of porous media properties has been regarded as a dominant factor

Accepted June 26, 2008

transport in the subsurface. This variability was also found crucial for assessing saturations and pressures of multiphase liquids in porous media. Thus it is expected that such variability would significantly impact LNAPL movement and spreading and the amount of mass lost from the NAPL body to the air phase as volatile contaminants or the water phase as dissolvable contaminants.

Stochastic analysis of multiphase flow in heterogeneous porous media was conducted using analytical methods based on the spectral, perturbation approach (e.g., Abdin and Kaluarachchi 1995; Chang et al. 1995 or numerical methods based on Monte Carlo approach (e.g., Essaid and Hess 1993; Abdin et al. 1995; Bradford et al. 1998; Zhu and Sykes 2000; Lemke and Abriola 2004; Yoon et al, 2007).

The objective of this study is to address the impacts of joint variability with and without correlation on LNAPL infiltration and movement in the vadose zone and the resulting air and water contaminant plumes.

Model Formulation and Governing Equations

The leakage of LNAPL through the vadose zone requires the treatment of three phases and the description of their mass balance as well as coupled movement. When the resulting contamination is considered, the mass of NAPL lost as a contaminant transferred to water and air is accounted for in the mass balance equations. The multiphase flow equations describe the mass balance for each of the three phases coupled with Darcy's law describing the flux of a particular constituent as a function of the pressure gradient. For both the air and water phases, the flow equation can be written in the form:

$$\frac{\partial}{\partial t}[\phi\, \rho_\alpha\, S_\alpha] = \sigma_\alpha + \nabla\left[\frac{k\, \rho_\alpha\, k_{r\alpha}}{\mu_\alpha}(\nabla P_\alpha + \rho_\alpha\, g\, \nabla Z)\right] \quad (1)$$

in which: the subscript α represents either water or air phase ("w" or "a"), ϕ is the porosity of the porous medium [dimensionless], S_α is the fluid volumetric saturation of phase α [dimensionless], σ represents a source or a sink of fluid [$ML^{-3}T^{-1}$], ρ is the fluid density [ML^{-3}], k is the intrinsic permeability [L^2], $k_{r\alpha}$ is the relative permeability for phase α, μ is the dynamic viscosity [$ML^{-1}T^{-1}$], P is the fluid pressure [$ML^{-1}T^{-2}$], g is the gravitational acceleration [LT^{-2}], and Z is the elevation [L].

A similar equation can be written for the NAPL, but the mass transfer terms should be added to the flux and source/sink terms. Thus for the NAPL phase (denoted by the subscript n), the flow equation is written as

$$\frac{\partial}{\partial t}[\phi\rho_n S_n] = \sigma_n + \nabla\left[\frac{k\rho_n k_{rn}}{\mu_n}(\nabla P_n + \rho_n g \nabla Z)\right] - \phi S_n \lambda_d (C^w_{nm} - C^w_n) - \phi S_n \lambda_v (C^a_{nm} - C^a_n) \quad (2)$$

in which: λ_d is the dissolution rate λ_v is the mass transfer rate for contaminant in air [T^{-1}], C^w_n is the concentration of contaminant dissolved [ML^{-3}], C^a_n is the concentration of contaminant volatilized [ML^{-3}], and C_{wm} and C_{am} are the equilibrium concentrations of

contaminant in water and air, respectively [ML^{-3}]. The equilibrium concentrations set a maximum limit to the ability of water and air to absorb dissolvable and volatile contaminants.

The flow equations of the three phases are linked by the capillary pressures. These capillary pressures are described by van Genuchten relationships, which express the functional relationships between saturations of the different phases and the capillary pressures (Van Genuchten, 1980). The dependence of the relative permeability of a certain phase on that phase saturation was taken similar to the formulations of Parker et al. (1987). The transport equations for the dissolved and volatilized contaminants were written in a similar manner to the equations of Sleep and Sykes (1989). The mass balance equation for the dissolved contaminant is thus written as

$$\frac{\partial}{\partial t}\left[\phi S_w C_n^w + k_d \rho_b C_n^w\right] = \frac{C_n^w}{\rho_w}\sigma_w + \nabla\left[\frac{kC_n^w k_{rw}}{\mu_w}(\nabla P_w + \rho_w g \nabla Z) + D_n^w \nabla\left(\phi S_w C_n^w\right)\right] + \phi S_w \lambda_d (C_{wm} - C_n^w) - \phi S_a \lambda_h (HC_n^w - C_n^a) \quad (3)$$

in which: k_d is the partition coefficient describing the mass partitioning between the liquid phase (water) and the solid phase (soil particles), ρ_b is the bulk density of the aquifer material [ML^{-3}], H is the dimensionless Henry's law constant, λ_h is mass transfer rate coefficient between water and air [T^{-1}], and D_n^w is the hydrodynamic dispersion coefficient for contaminant dissolved in the water phase [L^2T^{-1}].

For the volatilized contaminant, the mass balance equation is written as

$$\frac{\partial}{\partial t}\left[\phi S_a C_n^a\right] = \frac{C_n^a}{\rho_a}\sigma_a + \nabla\left[\frac{kC_n^a k_{ra}}{\mu_a}(\nabla P_a + \rho_a g \nabla Z) + D_n^a \nabla\left(\phi S_a C_n^a\right)\right] + \phi S_a \lambda_v (C_{wm} - C_n^a) + \phi S_a \lambda_h (HC_n^w - C_n^a) \quad (4)$$

in which: D_n^a is the hydrodynamic dispersion coefficient for volatile contaminant in the air phase [L^2T^{-1}] and all the other symbols are as defined earlier. Similar to the mass balance equation for the contaminant dissolved in the water phase, the equation of the volatile contaminant has two mass transfer processes: the mass gained from the NAPL body and mass transfer with the water phase. When the latter acts as a source for air contamination, the contaminant has to first dissolve in the water phase and subsequently vaporize and move to the air phase. The volatile contaminant in the air phase can also be lost within the domain to the water phase and can leave the model domain across the boundaries.

The mathematical model is composed of the five coupled partial differential equations (Eqs. 1 through 4) and a set of auxiliary equations relating capillary pressures to saturations and relative permeabilities to saturations. These equations cannot be solved analytically except for very simplified cases and under many restrictive assumptions. Here, we employ a numerical solution using block-centered finite differences with a forward time central space scheme (FTCS) discretization and an implicit pressure explicit saturation (IMPES) solution procedure (Peaceman, 1977).

The discretized equations and the IMPES scheme result in four equations being converted into linear systems of equations and solved using an algebraic multi-grid (AMG) solver (Stuben, 2001), and the remaining equation is solved explicitly.

To determine the spatial varability patterns of van Genuchten parameters, α (between water and air) and n, Essaid and Hess (1993) obtained relationships by trail and error to yield estimates of α and n that match particle-size estimated retention curves.

Simulation Domain and Initial and Boundary Conditions

A two-dimensional vertical domain of dimensions 100 m × 15 m is selected for implementing the solution of the multiphase flow equations and contaminant transport equations (Fig. 1). Homogeneous conditions were assumed in the subsequent simulations. The two-dimensional domain was divided into a uniform grid of square blocks of length $\Delta x = \Delta z$. The size of each grid cell was 0.25 m × 0.25 m with a total number of 24,000 cells (60 rows×400 columns). Initial and boundary conditions were identified for both the vadose zone portion and the saturated zone portion of the simulation domain. The multiphase flow problem requires specification of initial values of saturations and pressures for all phases. To get these initial values, the multiphase flow equations for water and air only were solved in a steady state condition with the assumption that NAPL did not exist in the domain initially before leakage. This gave an initial distribution for air and water saturations and the corresponding pressures. For contaminant transport equations, it was assumed that subsurface water and air were free of contamination before leakage and thus the values of dissolved and volatilized contaminants were set equal to zero. The boundary conditions for the multiphase flow problem and the associated transport problem are shown in Fig. 1.

Results and Discussion

The simulations presented here are conducted in a Monte Carlo framework where 1000 realizations are generated for each of the cases studied. The multiphase flow problem and the associated contaminant transport problem were solved for each of these realizations and the ensemble of the results was subsequently analyzed. Nine cases were considered with different sources of heterogeneities and different correlation cases. The purpose was to examine the effects of heterogeneities in porous medium parameters on LNAPL migration and spreading, mass transfer, and transport processes. Table 1 summarizes the different cases considered where in the first three cases, only one parameter (considering the van Genuchten parameters set as one parameter) is spatially varying and the others are kept uniform at their mean value. Cases 4-6 deal with deterministic porosity but the intrinsic permeability and the van Genuchten parameters are both spatially varying with positive correlation (Case 4),

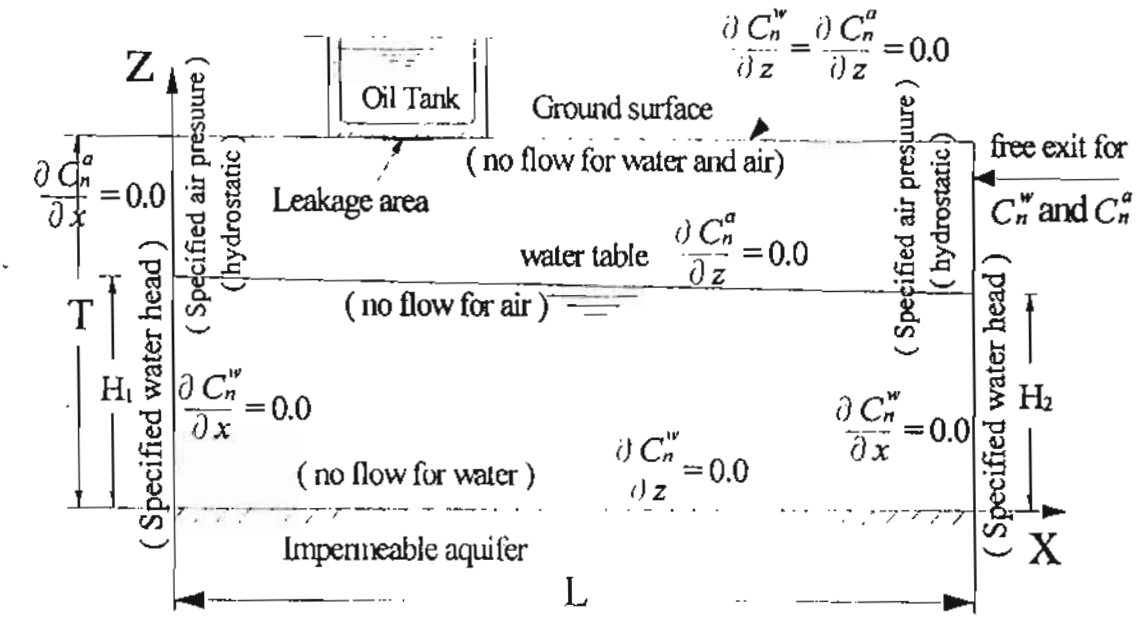

Fig. 1 Domain outline and boundary conditions for (a) the multiphase flow problem, and (b) the contaminant transport problem.

negative correlation (Case 5), or no correlation (Case 6). Similarly, Cases 7-9 consider deterministic van Genuchten parameters but heterogeneous permeability and porosity with positive correlation (Case 7), negative correlation (case 8), and no correlation (Case 9). In each case, 1000 realizations of a statistically homogeneous aquifer are generated for the varying parameters.

Figure 2 shows the distributions of NAPL saturations after 80 days from beginning of leakage for the homogeneous case (reference case) with uniform mean properties. The figure also shows the ensample mean of 1000 realizations for each of the nine cases of the heterogeneity scenarios. One can see that the heterogeneity in van Genuchten parameters and porosity has a negligible effect on saturation of NAPL but the heterogeneity in intrinsic permeability has a noticeable effect on increasing the LNAPL spreading and decreasing its maximum saturation. The dissolved contaminant resulting in each of the cases has a wide range of values and thus it is convenient to present the concentration value using logarithmic scale. Figure 3 displays the dissolved plumes where Log C_n^w with C_n^w being in gm/m^3 is contoured for the ensemble mean in the nine cases, and the result for the homogeneous case is also displayed in the figure. It is clear from Figure 3 that the heterogeneity of intrinsic permeability plays a major role in the movement and dispersion of the dissolved contaminant plume. The

cases that has heterogeneous permeability lead to more spreading and longer lateral and vertical travel distances compared to the homogeneous case. However, when k is deterministic the mean dissolved plume looks very similar to the homogeneous case despite the heterogeneity of porosity and van Genuchten parameters.

Figure 4 shows the ensemble mean distribution of volatilized contaminant concentration in the vadose zone above water table. Again, values of concentrations in gm/m^3 are contoured in logarithmic scale for both the homogeneous and heterogeneous cases. The spreading of volatilized contaminants is also wider for the heterogeneous cases than for the homogeneous case. Similar to their effect on the dissolved contaminant plume, the heterogeneities in van Genuchten parameters and porosity have a negligible effect on the volatilization pattern in comparison to the homogeneous case (compares cases 2 and 3 to the homogeneous case in Figure 4). The NAPL mass within the domain is distributed among three components: the NAPL body, the dissolved contaminants in the water phase and the volatilized contaminants in the air phase. The change of the last two components as time progresses is shown in Figure 5 for a total simulation time of 80 days. Figure 5 shows the comparison between homogeneous case and the different cases of heterogeneity in terms of the total dissolved mass and the total volatilized mass. At early times there are no differences among the heterogeneity cases and the homogeneous case. As time progresses minor differences start to appear and slightly increase with time.To represent the plume (NAPL and dissolved contaminant) movement and dispersion, spatial moments are calculated for the ensemble mean plume in each one of the heterogeneity cases. These spatial moments for the NAPL plume are computed as:

$$X_i = \frac{\iint_{R^2} \phi \bar{S}_n(x_1, x_2)\, x_i\, dx_1 dx_2}{\iint_{R^2} \phi \bar{S}_n(x_1, x_2)\, dx_1 dx_2} \quad i = 1,2 \tag{5}$$

$$L_{cg} = \sqrt{X_1^2 + X_2^2} \tag{6}$$

$$X_{ii} = \frac{\iint_{R^2} \phi \bar{S}_n(x_1, x_2)(x_i - X_i)^2\, dx_1 dx_2}{\iint_{R^2} \phi \bar{S}_n(x_1, x_2)\, dx_1 dx_2} \quad i = 1,2 \tag{7}$$

in which: X_i is the first spatial moment in the x_i direction, X_{ii} is the second spatial moment in the x_i direction, and L_{cg} is the distance from the middle point of the leakage source to the NAPL plume center of mass, and $\bar{S}_n(x_1, x_2)$ is the ensemble mean saturation of the NAPL plume at spatial location (x_1, x_2). To determine X_i, it may be convenient to take the origin as the center point of the leakage source. By doing so, L_{cg} represents the distance NAPL or the contaminant traveled from the start of the simulation to the time at which the moments were obtained. Similar expressions can be written for the dissolved contaminant plume moments.

Figure 6a exhibits the variation of the NAPL travel distance, L_{cg}, and the

second spatial moment in the horizontal and vertical directions, X_{11} and X_{22}, for the homogeneous and heterogeneous cases. It is clear that the NAPL plume spreading is larger in the horizontal direction than the vertical direction. Also, it can be seen that there is no significant differences among the heterogeneous cases and between them and the homogeneous case. Thus it can be concluded that the porous medium heterogeneity does not impact the NAPL movement or spreading regardless of the heterogeneity type or any imposed correlations. This is because of the continuous leakage source assumed in these simulations.

Figure 6b displays the ensemble plume travel distance, L_{cg}, for the dissolved contaminant. All heterogeneity cases had the same movement rate which was faster than the homogeneous case. As a result, the travel distance was almost the same in all heterogeneous cases and was longer for these cases than for the homogeneous case.

Figure 7 shows the spatial moments, X_{11} and X_{22}, of the dissolved plume (the ensemble mean) which express the lateral and vertical spreading. Although the travel distance of the center of mass of the mean dissolved plume does not change among the heterogeneity cases (Figure 6b), the lateral spreading is different between the heterogeneous cases and is larger than the homogeneous case (Figure 7a). Cases 2 and 3 with homogeneous intrinsic permeability but random van Genuchten parameters or porosity yield less spreading than the other heterogeneity cases. Case 8 with negative correlation between porosity and intrinsic permeability exhibits more lateral spreading than all other cases. On the other hand, Case 7 with positive correlation between porosity and intrinsic permeability shows less lateral spreading than all heterogeneity cases involving heterogeneous permeability. When porosity and intrinsic permeability were positively correlated, the resulting velocity field has less variability than if porosity was uniform. Conversely, when negative correlation was imposed the resulting velocity field experienced by the dissolved plume had more variability than if porosity was uniform. This explained the increased spreading of Case 8 and the decreased spreading of Case 7.

Figure 7b displays the second spatial moments in the vertical direction. Minor differences exist between the cases involving heterogeneous permeability. Cases 2 and 3 with homogeneous permeability yield smaller second moments at late times. However, the moments for the heterogeneous cases were much larger than the homogeneous case.

Conclusions

This work presents two-dimensional simulations of oil infiltration (from ground storage tanks for example) into heterogeneous aquifers and the resulting air and water contamination. Nine simulation cases were conducted with different heterogeneity scenarios taking into account the heterogeneity of main soil properties (intrinsic

permeability, porosity, and van Genuchten parameters) in a stochastic Monte Carlo frame with positive, negative, and no correlation between

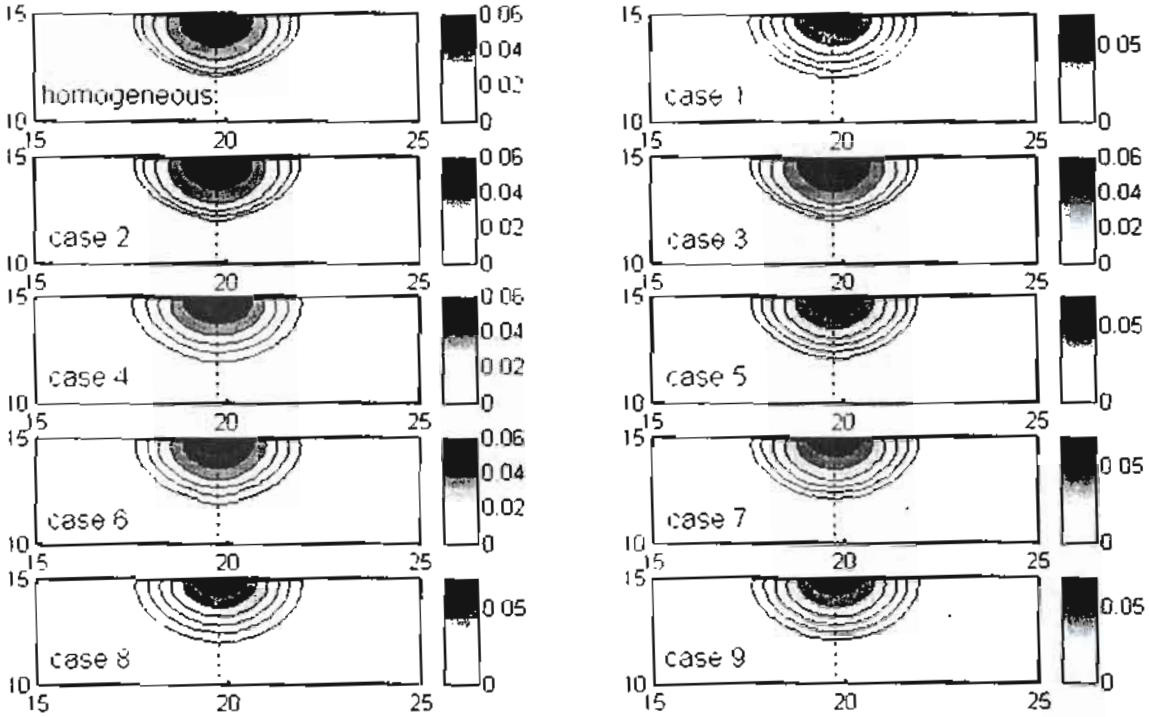

Figure 2: Saturation of NAPL in the domain after 80 days for the homogeneous case and the ensample mean of the heterogeneous cases.

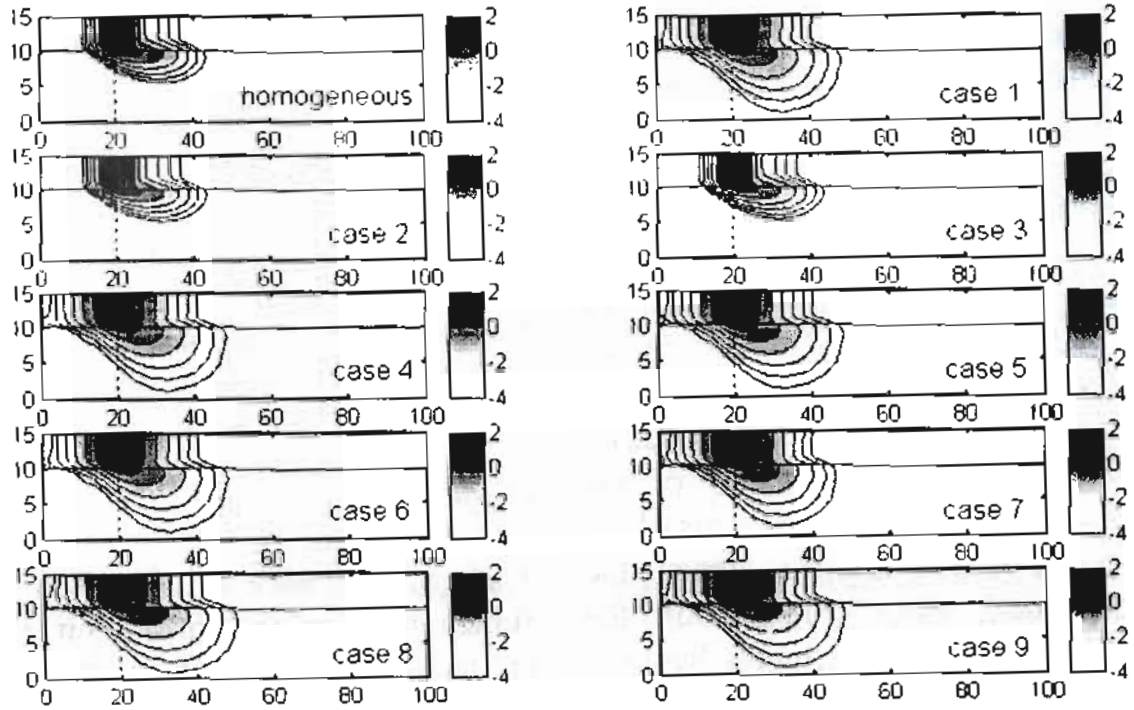

Figure 3: Dissolved contaminant ($\mathrm{Log}\,C_n^w$) distribution in the domain after 80 days for the homogeneous case and the ensample mean of the heterogeneous cases.

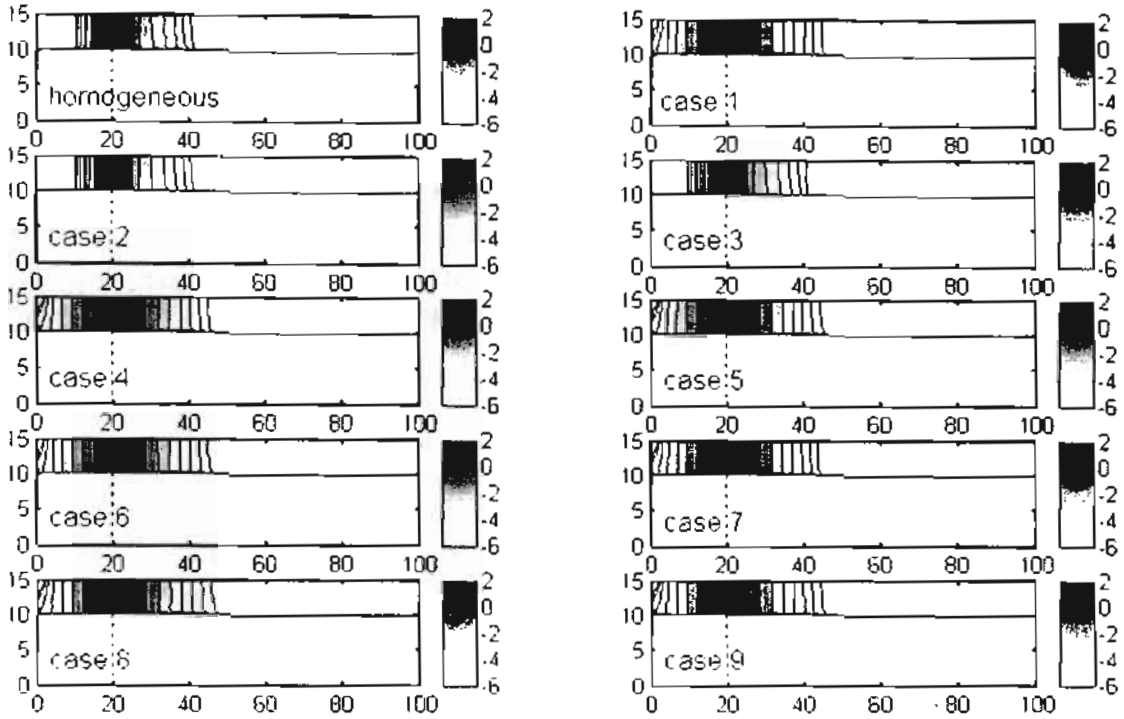

Figure 4: Volatilized contaminant (Log C_v'') distribution in the domain after 80 days for the homogeneous case and the ensample mean of the heterogeneous cases.

parameters. The results illustrate that the spatial heterogeneity of any of the considered parameters have very little impact on the NAPL saturations and spreading pattern. This was probably due to the continuous leakage scenario considered in all simulations presented in this study. Also, the spatial variability of porosity and van Genuchten parameters slightly impact the lateral spreading pattern of the dissolved contaminant plume. On the other hand, the heterogeneity of intrinsic permeability had a large effect on the dissolved and volatilized contaminants' movement and spreading. A homogeneous case was considered but using uncertain intrinsic permeability distribution. This case shows that the value of the permeability significantly impacts the NAPL, dissolved and volatilized contaminant patterns. This indicates that in practical applications, it is more important to develop an accurate effective permeability value than to characterize its spatial variability in order to appropriately model LNAPL leakage and associated contamination.

References

- Abdin AE, Kaluarachchi JJ, Kemblowski MW, Chang C-M (1995) Stochastic analysis of two-phase flow in porous media: II, Comparison between perturbation and Monte Carlo results. Transp Porous Media 19:261-280.

18(1):359-367.

- Bradford SA, Abriola LM, Rathfelder KM (1998) Flow and entrapment of dense nonaqueous phase liquids in physically and chemically heterogeneous aquifer formations. Adv Water Resour 22(2):117-132.

- Chang C-M, Kemblowski MW, Kaluarachchi JJ, Abdin AE (1995) Stochastic analysis of two-phase flow in porous media: 1. Spectral/perturbation approach. Transp Porous Media 19: 233-259.

- Corapcioglu MY, Tuncay K, Celyan BK (1996) Oil mound spreading and migration with ambient groundwater flow in coarse porous media. Water Resour Res 32(5):1299-1308.

- Essaid HI, Hess KM (1993) Monte Carlo simulation of multiphase flow incorporating spatial variability of hydraulic properties. Ground Water 31(1):123-134.

- Kaluarachchi JJ, Parker JC (1989) An efficient finite element method for modeling multiphase flow. Water Resour Res 25(1): 43-54.

- Kim J, Corapcioglu MY (2001) Sharp interface modeling of LNAPL spreading and migration on the water table. Env Eng Sci

- Lemke LD, Abriola LM (2004) Dense nonaqueous phase liquid (DNAPL) source zone characterization: Influence of hydraulic property correlation on predictions of DNAPL infiltration and entrapment. Water Resour Res 40:1-16.

- Liao B, Aral MM (2000) Semi-analytical solution of two-dimensional sharp interface LNAPL transport models. J Cont Hydrol 44:203-221.

- Mendicino G, Senatore A, Spezzano G, Straface S (2006) Three-dimensional unsaturated flow modeling using cellular automata. Water Resour Res 42:1-18.

- Peaceman D. 1977 Fundamentals of Numerical Reservoir Simulation Elsevier, New York.

- Sleep BE, Sykes JF (1989) Modeling the transport of volatile organics in variably saturated media. Water Resour Res 25(1):81-92.

- Stuben K (2001) A Review of Algebraic Multigrid. J Comp App Math (JCAM) 128:281-309.

- Suk H, Yeh G (2007) 3D, three-phase flow simulations using the Lagrangian-Eulerian approach

with adaptively zooming and peak/valley capturing scheme. ASCE J Hydrol Eng 12(1):14-32.

- Van Genuchten MTh (1980) A closed form equation for predicting the hydraulic conductivity of unsaturated soils. Soil Sci Soc Am J 44:892-898.

- Yoon H, Valocchi AJ, Werth CJ (2007) Effect of soil moisture dynamics on dense nonaqueous phase liquid (DNAPL) spill zone architecture in heterogeneous porous media. J Cont Hydrol 90:159-183.

- Zhu J, Sykes JF (2000) Stochastic simulations of NAPL mass transport in variably saturated heterogeneous porous media. Transp Porous Media 39:289-314.

notched beams were investigated. The notch length to beam depth ratio was equal to 0.5. Test results showed brittle type of fracture in the case of PPFRC while the type of fracture changed to be more ductile with increasing steel fiber percent in the composite. Tensile and flexural

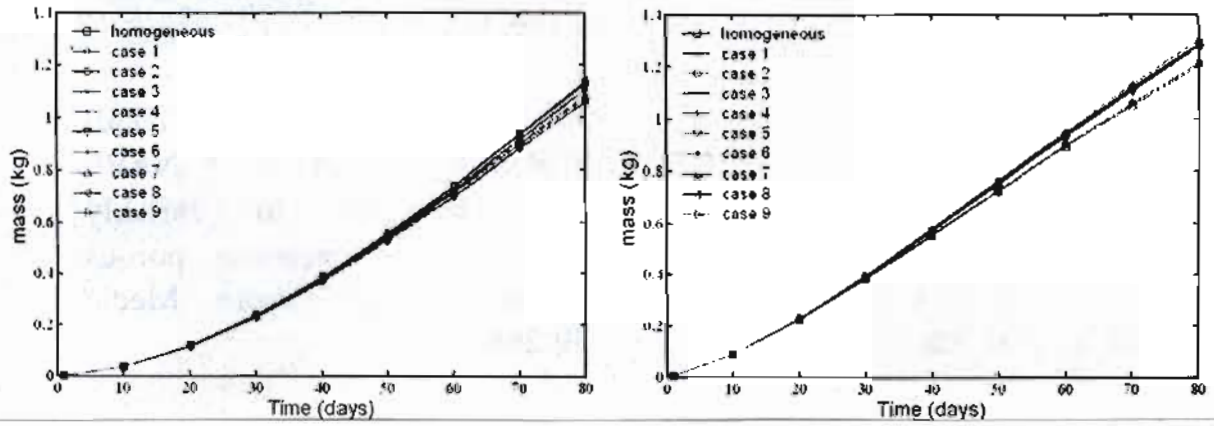

7. El Damatty, A. A., Abushagur, M and Yousse, M. A., (2003) "Experimental and analytical investigation of steel beams rehabilitated using GFRP sheets", Steel and Composite Structures, Vol. 3, No. 6, pp. 421-438.
8. Alghamdi, S. A., (2004) "On Analysis of Shear Lag In Steel Box-Girders, Fourteenth Engineering Mech., The University of Texas at Austin, USA, May 21-24.
9. Malcolm, D. J. and Redwood, R.G., (1970) "Shear Lag in Stiffened Box Girders," J. Struct. Div., Proc. ASCE, 96(ST7), pp 1403-14019.
10. Jin Cheng, C. S., Xiao, C. R., (2005) "Probabilistic shear-lag analysis of structures using Systematic RSM", Structural Engineering and Mechanics, Vol. 21, No. 5, pp. 507-518.